A Robust Time-Stepping Scheme for Quasistatic Rigid Multibody Systems

Tao Pang, Russ Tedrake

***Abstract*— An effective scheme to simulate low-speed, contact-rich manipulation tasks is to assume quasistatic physics and advance system states by solving linear complementarity problems (LCPs). However, the existing LCP-based quasistatic time-stepping scheme fails to simulate grasping—an essential motion primitive in manipulation—due to two drawbacks specific to quasistatic systems. Firstly, inputs to quasistatic systems are velocity commands instead of torques. This can lead to penetration, and thus an infeasible LCP, when two rigid bodies in contact are commanded to push against each other. Secondly, as multiple force solutions exist for a given velocity command, a grasping velocity command is not guaranteed to generate sufficient grasping forces. In this paper, we reformulate the quasistatic time-stepping scheme as an optimization problem with complementarity constraints and a quadratic objective. By minimizing the difference between actual and commanded velocities, linearized non-penetration constraints can always be satisfied. Moreover, undesirable solutions with insufficient normal forces can be removed by considering elasticity, which is modeled by comparing actual and commanded velocities. The resulting optimization problem is a mixed-integer quadratic program, which can be solved reasonably quickly for small-to-medium-sized systems. The effectiveness of the proposed reformulation is validated by simulation results of systems with different levels of complexity.**

I. Introduction

Time-stepping schemes based on kinematic models [1] have been used to quickly simulate robotic manipulation tasks, and are easy to implement. Given the current system configuration, such a kinematic time-stepping scheme computes the system configuration at the next time step subject to kinematic constraints. However, kinematic time-stepping schemes lack the ability to reason about forces. As a result, such simulators can only handle contacts by fixing two objects together when one is in close proximity to the other.

As robotic manipulation typically involves making and breaking contact, forces, especially contact forces, are essential in simulating manipulation tasks. For instance, after a robotic gripper executes a force-closure grasp on an object, the object moves together with the gripper without slippage only if the contact forces are sufficiently large. In contrast, slippage would occur when external wrenches acting on the object overwhelm the grasping wrench. Moreover, contact forces also play an indispensable role in nonphrehensile manipulation [2], which extends the workspace of manipulators by leveraging external interactions.

Computer Science and Artificial Intelligence Laboratory, Massachusetts Institute of Technology, 77 Massachusetts Avenue, Cambridge, MA 02139. pangtao,russt@mit.edu

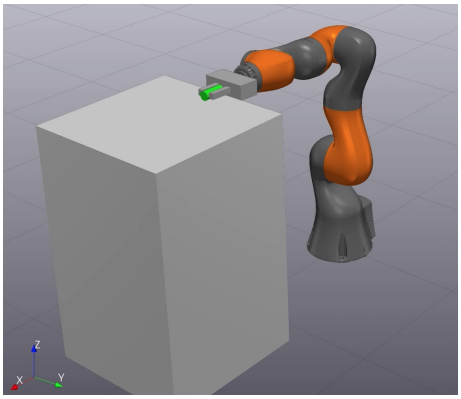

Fig. 1: Grasping of an object by a robotic arm with a parallel-jaw gripper.

Employing quasistatic models enables simulators to reason about forces without adding too much complexity. Quasistatic models take into account forces which are significant for low-speed multibody interactions (such as friction and gravity), but at the same time keep only half as many states (configuration only) as their full-fledged dynamic counterparts. Although inertial and Coriolis forces are ignored, quasistatic models have proven to be sufficiently accurate for low-speed multibody systems, and have been used in manipulation research with great success. Pushing an object having planar contact with its supporting surface has been extensively studied in the 1990s [3], [4], [5], [6]. More recently, Hogan and Rodriguez developed an experimentally-verified single-contact push controller based on quasistatic models [7]. Zhou *et al.* proposed a quasistatic simulation framework that reproduces the stochasticity observed in 2-dimensional (2D) sliding [8]. Despite its rich history in manipulation, quasistatic models have been used almost exclusively in the simulation of pushing, but not grasping (Figure 1).

Modeling contact and friction using linear complementarity problems (LCPs) has emerged as an efficient method to resolve contact forces when simulating multibody systems [9], [10]. Such systems are hybrid in the sense that the sysem dynamics changes in different contact modes, the nubmer of which grows exponentially with the number of bodies and possible contact points. As a result, resolving contact by explicitly enumerating contact modes quickly becomes intractable in contact-rich scenarios such as robotic manipulation [11]. In contrast, by encoding contact and friction implicitly as complementarity constraints, complementarity-

based time-stepping schemes avoid explicit enumeration, and are thus more suitable to simulation of contact-rich, multibody interactions.

In this paper, we propose a robust complementarity-based quasistatic simulation framework for manipulation tasks. Leveraging the efficiency of LCP in resolving contacts, the proposed framework extends kinematic time-stepping schemes by reasoning about contact forces, while adding minimum complexity.

The rest of the paper is organized as follows: Section II reviews related work; Section III summarizes the modeling of quasistatic multibody systems with contact and friction; Section IV illustrates our proposed improvements to existing quasistatic LCP time-stepping schemes; examples validating the effectiveness of the proposed reformulation are presented in Section V.

II. Background

Assuming a quasistatic model and Coulomb friction, Mason studied planar pushing without a detailed model of the pressure distribution between the object and its supporting surface, and derived the voting theorem, which predicts the sense of rotation of an object being pushed at a single contact point [4]. Also under the condition of unknown pressure distribution, Lynch and Mason proposed a 2D pushing planner capable of generating obstacle-avoiding paths by chaining together *stable pushes*—motion primitives that ensure the object remains fixed to the manipulator while being pushed [5].

It turns out that planning and control of planar pushing can be made less conservative by utilizing the pressure distribution between surfaces. First proposed by Goyal [12], the limit surface, a convex surface that bounds all possible friction forces and moments, has been widely used to model such pressure distributions. The mathematical expression of limit surfaces can be greatly simplified using an ellipsoidal approximation [6], which forms the basis of several feedback controllers for single-point planar pushing [3], [7]. Recently, Zhou further improved the fidelity of limit surface approximations by fitting a sum-of-squares polynomial to experimental data [13]. Although approaches that reason about planar surface-to-surface contact work extremely well for planar pushing, they do not easily generalize to 3D multi-contact scenarios.

Another line of work that does naturally handle 3D multibody interactions uses complementarity to model contact and friction. In the dynamic time-stepping scheme developed by Stewart and Trinkle [9], the states of a dynamical system are first expressed in terms of the contact forces through Newton's 2nd law. As either the distance or the force between two bodies has to be zero, complementarity constraints can then be added to the contact forces to form an LCP, which is solved to obtain the contact forces and system states at the next time step. Trinkle later proposed a quasistatic time-stepping scheme which uses similar complementarity constraints as the dynamic scheme, but replaces Newton's 2nd law with a simpler force balance constraint [14].

Although LCP does generalize quasistatic models to 3D, it still cannot handle grasping simulation. As inertial effects are ignored under the quasistatic assumption, the states of a quasistatic system are advanced by inputs in the form of velocity commands instead of torques. In time-stepping simulations, this makes penetration difficult to avoid when two rigid bodies are in contact (e.g. when an object is grasped). For example, consider a parallel-jaw gripper trying to grasp a cylinder, as shown in Figure 2. In dynamic simulations, torque commands apply forces on both fingers of the gripper. When both fingers are in contact with the cylinder (position 2), there is no problem commanding nonzero forces on the fingers because the forces would simply translate into the cylinder's acceleration. In contrast, the *displacement* of fingers are commanded in a quasistatic simulation. If nonzero displacement is commanded at position 2, the fingers would penetrate the cylinder (position 3) and make the LCP infeasible.

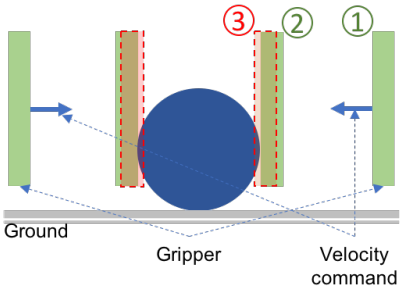

Fig. 2: 2D parallel-jaw gripper picking up a cylinder. Initially at position 1, the gripper moves towards the cylinder following the velocity command. The cylinder is grasped when the gripper reaches position 2. If continuing to follow the velocity command, the gripper would be at position 3 and cause penetration.

Moreover, even if the velocity command drops to zero right after the gripper grasps the cylinder and before penetration occurs, zero or small normal forces between the gripper and the cylinder are usually a feasible solution to the LCP. Without sufficiently large normal forces, the grasped object will simply slip out of grasp when the gripper moves up.

In this paper, we present a mixed-integer quadratic program (MIQP) reformulation of Trinkle's quasistatic time-stepping LCP scheme. The complementarity constraints are first converted into linear constraints with binary varaibles using the big-M formulation. By setting the objective as minimizing the norm of the difference between the velocity command and the actual actuator velocity, the MIQP formulation is able to "softly" follow the velocity command while maintaining feasibility. Moreover, elasticity can be modeled by adding normal force lower bounds that are proportional to the amount of "squeezing" generated by the velocity command. The lower bounds remove solutions whose normal forces are small, and guarantee that the object can be picked up when the velocity command "squeezes" the object hard enough.

III. Quasistatic Multibody System with Contact

Primarily based on [14], this section summarizes the definition of quasistatic systems and the complementarity constraints commonly used to model contact and friction.

A. Quasistatic representation of a multibody system

Let $q(t) = \begin{bmatrix} q_u^T(t) & q_a^T(t) \end{bmatrix}^T \in \mathbb{R}^{n_q}$ be the configuration of a multibody system with $q_u(t) \in \mathbb{R}^{n_u}$ being the unactuated degrees of freedoms (DOFs) and $q_a(t) \in \mathbb{R}^{n_a}$ the actuated DOFs. For example, in a system with a robotic arm and an object that the arm tries to pick up, q_u is the pose of the object and q_a consists of the joint angles of the robotic arm.

The generalized velocity of the system can be similarly partitioned into actuated and unactuated segments: $v(t) = \begin{bmatrix} v_u^T(t) & v_a^T(t) \end{bmatrix}^T \in \mathbb{R}^{n_v}$. As q may live on a manifold (for example, when quaternions are used to represent orientation), $v \neq \dot{q}$ in general, but is related to $\dot{q}$ by a linear transformation: $v = G(q)\dot{q}$, where $G(q) \in \mathbb{R}^{n_v \times n_q}$.

A generic discrete dynamical system has the form $x\left((l+1)h\right) = f(x(lh), w(lh))$, where x is the system state, w the input, l the current time step and h the step size. For a quasistatic system, $x := q$ and $w := \bar{v}_a$, where the overscore signifies the fact that the input is the prescribed velocity of the actuated DOFs, which could be different from the actual actuated velocity v_a.

B. Contact kinematics

Let q and v be the configuration and generalized velocity of a multibody system, as defined in Section III-A. Denote by n_c the number of conact pairs in the system, and consider the contact pair indexed by i ($i \in \{1 \dots n_c\}$), which involves two rigid bodies denoted by A and B, as shown in Figure 3. There exist efficient algorithms (such as [15]) that can find $\phi_i(q)$, the signed distance function between A and B, together with a pair of points (α, β), α fixed to body A and β to B, such that

$$|\phi_i(q)| = \| {}^O\boldsymbol{x_\alpha} - {}^O\boldsymbol{x_\beta} \|, \tag{1}$$

where ${}^O\boldsymbol{x_\alpha}$, ${}^O\boldsymbol{x_\beta} \in \mathbb{R}^3$ are the coordinates of α and β expressed in reference frame Ψ_O. ${}^O\boldsymbol{v_\alpha}$ and ${}^O\boldsymbol{v_\beta}$, the velocity of α and β in Ψ_O, can be obtained with forward kinematics [16], [17].

We define $\boldsymbol{n_i}$, the contact normal of contact i, as the unit vector pointing from α to β. We also define $\boldsymbol{d_i} = [\boldsymbol{d_{i1}}, \dots, \boldsymbol{d_{i(n_{d_i})}}] \in \mathbb{R}^{3 \times n_{d_i}}$, where the $\boldsymbol{d_{ij}}$'s constitute a set of unit basis vectors that positively span the tangent plane.

The relative contact velocity $\boldsymbol{v_i}$ can be defined as

$$\boldsymbol{v_i} = {}^O\boldsymbol{v_\beta} - {}^O\boldsymbol{v_\alpha}. \tag{2}$$

It can be shown that $\boldsymbol{v_i} = J_{c_i}^v(q)v$, where $J_{c_i}^v(q) = \frac{\partial \boldsymbol{v_i}}{\partial v} \in \mathbb{R}^{3 \times n_v}$ is the contact Jacobian for contact i with respect to v [16].

The rate of change of $\phi_i(q)$ can be obtained by projecting $\boldsymbol{v_i}$ along $\boldsymbol{n_i}$:

$$\dot{\phi}_i = \boldsymbol{n_i}^T \boldsymbol{v_i} = \left(\boldsymbol{n_i}^T J_{c_i}^v(q)\right) v = J_{n_i}^v(q)v \tag{3}$$

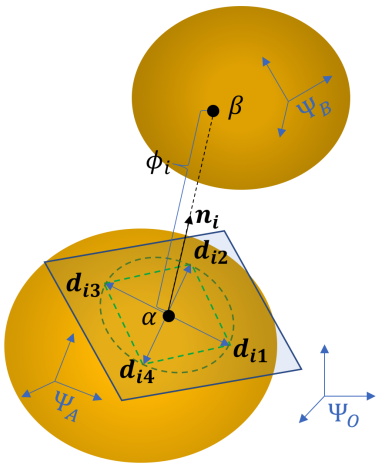

Fig. 3: Kinematics of contact pair i. Ψ_O: global reference frame. Ψ_A and Ψ_B: reference frames fixed to body A and B, respectively. $\boldsymbol{n_i}$: contact normal. $\boldsymbol{d_i} = [\boldsymbol{d_{i1}}, \boldsymbol{d_{i2}}, \boldsymbol{d_{i3}}, \boldsymbol{d_{i4}}]$: matrix of tangent vectors, $n_{d_i} = 4$.

Analogously, tangential sliding velocities, $\nu_i \in \mathbb{R}^{n_{d_i}}$, can be defined as the projection of $\boldsymbol{v_i}$ along the $\boldsymbol{d_{ij}}$'s:

$$\begin{aligned} \nu_i &= \begin{pmatrix} \nu_{i1} \\ \vdots \\ \nu_{i(n_{d_i})} \end{pmatrix} = \begin{pmatrix} \boldsymbol{d_{i1}^T} \\ \vdots \\ \boldsymbol{d_{i(n_{d_i})}^T} \end{pmatrix} \boldsymbol{v_i} \\ &= \left(\boldsymbol{d_i}^T J_{c_i}^v(q)\right) v = J_{f_i}^v(q)v \end{aligned} \tag{4}$$

Note that $\boldsymbol{d_i}$, the set of spanning vectors in the tangent plane, must be *balanced*, i.e. for every vector $\boldsymbol{d_{ij}} \in \boldsymbol{d_i}$, we also need $-\boldsymbol{d_{ij}} \in \boldsymbol{d_i}$.

$J_{n_i}^v$ and $J_{f_i}^v$ in (3) and (4) are the normal and tangential Jacobians for a single contact pair [1]. We can define the normal and tangential Jacobians for all contact pairs by concatenating $J_{n_i}^v$'s and $J_{f_i}^v$'s, i.e.

$$J_n^v = \begin{pmatrix} J_{n_1}^v \\ \vdots \\ J_{n_{n_c}}^v \end{pmatrix} \in \mathbb{R}^{n_c \times n_v}, J_f^v = \begin{pmatrix} J_{f_1}^v \\ \vdots \\ J_{f_{n_c}}^v \end{pmatrix} \in \mathbb{R}^{n_d \times n_v}, \tag{5}$$

where $n_d = \Sigma_i n_{d_i}$. Jacobians with respect to $\dot{q}$ can be obtained by post-multiplying J_*^v with G, i.e. $J_*^q = J_*^v G$.

C. Non-penetration constraint

Let $\phi, \lambda_n \in \mathbb{R}^{n_c}$ be vectors of signed minimum distances and normal contact forces for all contact pairs. A non-penetration constraint dictates that the signed distance between any pair of rigid bodies in the system must be non-negative, and that a non-zero normal contact force can exist at contact i if the two bodies are in contact ($\phi_i = 0$), which can be written succinctly as

$$0 \leq \phi(q) \perp \lambda_n \geq 0. \tag{6}$$

[1] For simplicity, the explicit dependency of Jacobians on q will be dropped from here onwards.

D. Force-balance constraint

The unactuated bodies in a quasistatic system are always in equilibrium, as inertial and Coriolis forces are negligible under the quasistatic assumption.

Assuming Coulomb friction for all contact pairs and inner-approximating the friction cone by a polyhedral cone [9], the contact force at contact i can be written as

$$\{\boldsymbol{n_i}\lambda_{n_i} + \boldsymbol{d_i}\lambda_{f_i} | \lambda_{n_i} \geq 0, \lambda_{f_i} \geq 0, \boldsymbol{e_i}^T\lambda_{f_i} \leq \mu\lambda_{n_i}\} \quad (7)$$

where $\lambda_{n_i} \in \mathbb{R}$ is the i-th component of λ_n, $\lambda_{f_i} \in \mathbb{R}^{n_{d_i}}$ consists of the components of friction force along the d_{ij}'s, and $\mathbf{e}_i = [1, 1, \ldots, 1]^T \in \mathbb{R}^{n_{d_i}}$.

The force balance condition in terms of generalized forces can thus be written as

$$J_n^{v_u T}\lambda_n + J_f^{v_u T}\lambda_f + \tau_u(q) = 0 \quad (8)$$

where $J_n^{v_u}$ and $J_f^{v_u}$ consist of columns of J_n^v and J_f^v corresponding to the unactuated generalized velocities v_u, and $\tau_u(q)$ is the lumped external generalized force vector that accounts for gravity, magnetism, etc..

E. Coulomb friction constraint

The Coulomb friction model makes the following assumptions about friction forces [12]:

- The contact force is inside the friction cone.
- When sliding, the direction of the friction force maximizes energy dissipation.

Under the polyhedral approximation of friction cones, the Coulomb friction model is equivalent to the following complementarity conditions [14]: for every contact i,

$$0 \leq (\gamma_i \mathbf{e}_i + \nu_i) \perp \lambda_{f_i} \geq 0, \quad (9)$$

$$0 \leq \mu\lambda_{n_i} - \boldsymbol{e_i}^T\lambda_{f_i} \perp \gamma_i \geq 0. \quad (10)$$

where γ_i is a slack variable whose numerical value typically equals $\|\nu_i\|$.

IV. Time-stepping MIQP Formulation

Given the system's configuration $q(lh)$ at the current time step l, a time-stepping method finds the system configuration at the next time step $q((l+1)h)$ by evaluating

$$\Delta q^l = q((l+1)h) - q(lh). \quad (11)$$

In this section, we explain how to construct an MIQP that solves for Δq^l subject to the constraints (6), (8), (9) and (10). We will use the shorthand notation q^l for $q(lh)$, where the superscript l denotes the time step at which $q(t)$ is evaluated.

A. Discretized constraints

Constraints (6), (8), (9) and (10) are *continuous-time* constraints, which means they involve system states and forces at an instantaneous t. In time-stepping simulations, however, system states and forces are only evaluated at *discrete* time steps. As a result, the continuous-time constraints are integrated over time steps and applied at the "knot" points $(t = 0, h, 2h, \ldots)$.

Accordingly, the non-penetration constraint (6) becomes

$$0 \leq \phi^{l+1} \perp P_{\lambda_n}^l \geq 0 \quad (12)$$

where $P_{\lambda_n}^l = \int_{lh}^{(l+1)h} \lambda_n(t)\,\mathrm{d}t$ is the impulse generated by normal contact forces $\lambda_n(t)$ over the time interval $t \in (lh, (l+1)h]$. The discretized non-penetration constraint implies that a nonzero impulse over $(lh, (l+1)h]$ exists at contact i only if the signed distance function evaluated at $t = (l+1)h$ is equal to zero, i.e. $P_{\lambda_{n_i}}^l > 0 \implies \phi_i^{l+1} = 0$. As $\phi(q)$ is usually a nonlinear function of q, its value at $t = (l+1)h$ is evaluated using its linearization about q^l:

$$\begin{aligned}\phi^{l+1} &= \phi^l + \left.\frac{\partial\phi}{\partial q_u}\right|_l \Delta q_u^l + \left.\frac{\partial\phi}{\partial q_a}\right|_l \Delta q_a^l \\ &= \phi^l + J_n^{q_u}|_l\,\Delta q_u^l + J_n^{q_a}|_l\,\Delta q_a^l.\end{aligned} \quad (13)$$

where the subscript l after the vertical bars means that the functions before the bars are evaluated at $t = lh$, and $J_n^{q_u}$ and $J_n^{q_a}$ consist of columns of J_n^q corresponding to q_u and q_a, respectively.

Similarly, constraint (9) becomes

$$0 \leq \left(\Gamma_i^l \mathbf{e}_i + \Psi_i^l\right) \perp P_{\lambda_{f_i}}^l \geq 0 \quad (14)$$

where $\Gamma_i^l = \gamma_i^l h$, $P_{\lambda_{f_i}}^l = \int_{lh}^{(l+1)h} \lambda_{f_i}(t)\,\mathrm{d}t$, and

$$\begin{aligned}\Psi_i^l = \nu_i^l h &= J_{f_i}^{q_u}\Big|_l (\dot{q}_u^l h) + J_{f_i}^{q_a}\Big|_l (\dot{q}_a^l h) \\ &= J_{f_i}^{q_u}\Big|_l \Delta q_u^l + J_{f_i}^{q_a}\Big|_l \Delta q_a^l.\end{aligned} \quad (15)$$

The discretized version of (9) and (10) for all contacts can thus be written as

$$0 \leq \underbrace{\left(E\Gamma^l + J_f^{q_u}\Big|_l \Delta q_u^l + J_f^{q_a}\Big|_l \Delta q_a^l\right)}_{\rho^l \text{ in (23)}} \perp P_{\lambda_f}^l \geq 0 \quad (16)$$

$$0 \leq \underbrace{UP_{\lambda_n}^l - E^T P_{\lambda_f}^l}_{s^l \text{ in (23)}} \perp \Gamma^l \geq 0 \quad (17)$$

where

$$E = \begin{pmatrix} \mathbf{e}_1 & 0 & \ldots & 0 \\ 0 & \mathbf{e}_2 & \ldots & 0 \\ \vdots & \vdots & \ddots & \vdots \\ 0 & 0 & \ldots & \mathbf{e}_{n_c} \end{pmatrix} \in \mathbb{R}^{n_d \times n_c}$$
$$U = \mathrm{diag}\left([\mu_1, \ldots, \mu_{n_c}]\right). \quad (18)$$

B. Avoiding penetration caused by velocity commands

Recall from Section III-A that the input to a quasistatic system is the velocity command $\bar{v}_a(t)$. Over one time step, the input is equivalent to $\Delta\bar{q}_a^l = hG(t)\bar{v}_a$.

In the LCP formulation, the Δq_a^l in (13) and (15) is directly substituted by $\Delta\bar{q}_a^l$. As a result, the LCP becomes infeasible if $\Delta\bar{q}_a^l$ causes penetration or constrains the system in such a way that the force balance constraints cannot be satisfied.

The violation of non-penetration constraints can be circumvented by adding new decision variables Δq_a which represent the actual change of the actuated DOFs. Δq_a^l is

allowed to be different from $\Delta\bar{q}_a^l$. If it was possible to add an objective to the mathematical program that minimizes $\|\Delta q_a^l - \Delta\bar{q}_a^l\|^2$, the actuated DOFs would follow the velocity command as closely as possible without violating the non-penetration constraints.

Although LCPs are feasibility problem that do not allow an objective function, complementarity constraints can be converted into linear constraints using binary variables, reformulating the LCP into an MIQP, which can be solved to global optimality.

A common technique for such conversions is the big-M method [18]. Consider the following generic complementarity condition:

$$0 \leq f(x) \perp g(x) \geq 0. \tag{19}$$

Using a binary variable z and a sufficiently large scalar M, (19) is equivalent to the following linear and binary constraints:

$$\begin{aligned} f(x) &\geq 0 \\ g(x) &\geq 0 \\ f(x) &\leq zM \\ g(x) &\leq (1-z)M \\ z &\in \{0,1\}. \end{aligned} \tag{20}$$

C. Removing undesirable solutions to the force balance constraints

Another issue with LCP-based quasistatic simulation is the existence of multiple solutions to the force balance constraints. For instance, in the cylinder pick-up example introduced in Figure 2, it is possible that the normal forces between the fingers and the cylinder are large enough so that friction between the fingers and the cylinder is able to balance the cylinder's weight, allowing the object to be picked up. It is equally possible that the normal forces are tiny, and as a result the cylinder needs the support force from the ground to remain in force balance. The existence of multiple solutions is actually a defect of the rigid body assumption. In reality, the cylinder deforms under the compression forces from the fingers. The more the cylinder deforms, the greater the normal force between the cylinder and the fingers.

In general, undesirable solutions with tiny normal forces can be removed by accounting for the object's elasticity. To that end, we first evaluate the linearized signed distance function from Equation 13 with Δq_a^l replaced by $\Delta\bar{q}_a^l$:

$$\bar{\phi}^{l+1} = \phi^l + J_n^{q_u}|_l \, \Delta q_u^l + J_n^{q_a}|_l \, \Delta\bar{q}_a^l. \tag{21}$$

We call $\bar{\phi}^{l+1}$ the *hypothetical penetration*, which represents the penetration that would have occurred had the velocity command $\Delta\bar{q}_a^l$ been strictly followed. When constructing the MIQP, average normal forces over a time step are given lower bounds proportional to the hypothetical penetration:

$$P_{\lambda_{n_i}}^l / h \geq -K_i \bar{\phi}_i^{l+1}. \tag{22}$$

This constraint is equivalent to attaching springs to the object's otherwise rigid surface. The spring at contact i has a rest length of $\bar{\phi}_i^{l+1}$ and stiffness K_i. If $\bar{\phi}_i \geq 0$, the added lower bound is negative, which is trivial because all normal forces are already bounded below by 0 (Equation (6)). In contrast, the lower bound becomes nontrivial when $\bar{\phi}_i \leq 0$. Moreover, the lower bound grows as $\Delta\bar{q}_a^l$ increases, reflecting the fact that the normal forces are larger when the fingers pinch the object harder.

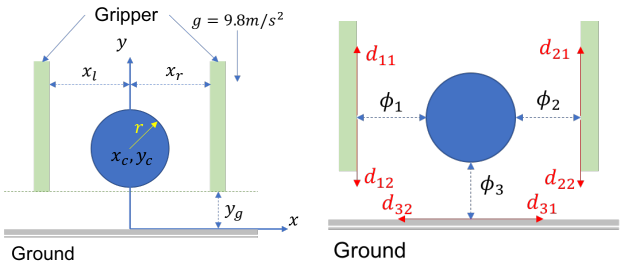

(a) System configuration (b) Normal distance functions and tangent vectors

Fig. 4: Parallel gripper picking up a cylinder

D. Summary

The MIQP formulation of the quasistatic time-stepping simulation scheme is summarized below:

$$\underset{\Delta q_u^l, \Delta q_a^l, P_{\lambda_n}^l, P_{\lambda_f}^l, \gamma^l, (z_i)_{i\in\{1,\ldots,N\}}}{\text{minimize}} \quad \|\Delta q_a^l - \Delta\bar{q}_a^l\|^2$$

subject to

$$(J_n^{v_u}|_l)^T P_{\lambda_n}^l + \left(J_f^{v_u}\Big|_l\right)^T P_{\lambda_f}^l + P_{\tau_u}^l = 0 \tag{23a}$$

$$\begin{pmatrix} \phi_n^{l+1} \\ \rho^l \\ s^l \end{pmatrix} = R \begin{pmatrix} \Delta q_u^l \\ \Delta q_a^l \\ P_{\lambda_n}^l \\ P_{\lambda_f}^l \\ \Gamma^l \end{pmatrix} + b, \tag{23b}$$

$$\begin{pmatrix} \phi_n^{l+1} \\ \rho^l \\ s^l \end{pmatrix} \geq 0, \begin{pmatrix} P_{\lambda_n}^l \\ P_{\lambda_f}^l \\ \Gamma^l \end{pmatrix} \geq 0, \tag{23c}$$

$$\begin{pmatrix} \phi_n^{l+1} \\ \rho^l \\ s^l \end{pmatrix} \leq M \begin{pmatrix} z_1 \\ \vdots \\ z_N \end{pmatrix}, \begin{pmatrix} P_{\lambda_n}^l \\ P_{\lambda_f}^l \\ \Gamma^l \end{pmatrix} \leq M \begin{pmatrix} 1-z_1 \\ \vdots \\ 1-z_N \end{pmatrix}, \tag{23d}$$

$$z_i \in \{0,1\}, i = 1 \ldots N, \tag{23e}$$

$$P_{\lambda_{n_i}}^l / h \geq -K_i \bar{\phi}_i^{l+1}, \tag{23f}$$

where $N = 2n_c + n_d$,

$\bar{\phi}^{l+1} = \phi^l + J_n^{q_u}|_l \, \Delta q_u^l + J_n^{q_a}|_l \, \Delta\bar{q}_a^l$, and

$$R = \begin{pmatrix} J_n^{q_u}|_l & J_n^{q_a}|_l & 0 & 0 & 0 \\ J_f^{q_u}\Big|_l & J_f^{q_a}\Big|_l & 0 & 0 & E \\ 0 & 0 & U & -E^T & 0 \end{pmatrix}, b = \begin{pmatrix} \phi^l \\ 0 \\ 0 \end{pmatrix}.$$

V. Examples

A. Grasping a cylinder with a 2D parallel gripper

To illustrate the improvements over Trinkle's LCP time-stepping scheme [14], we reconsider the problem introduced

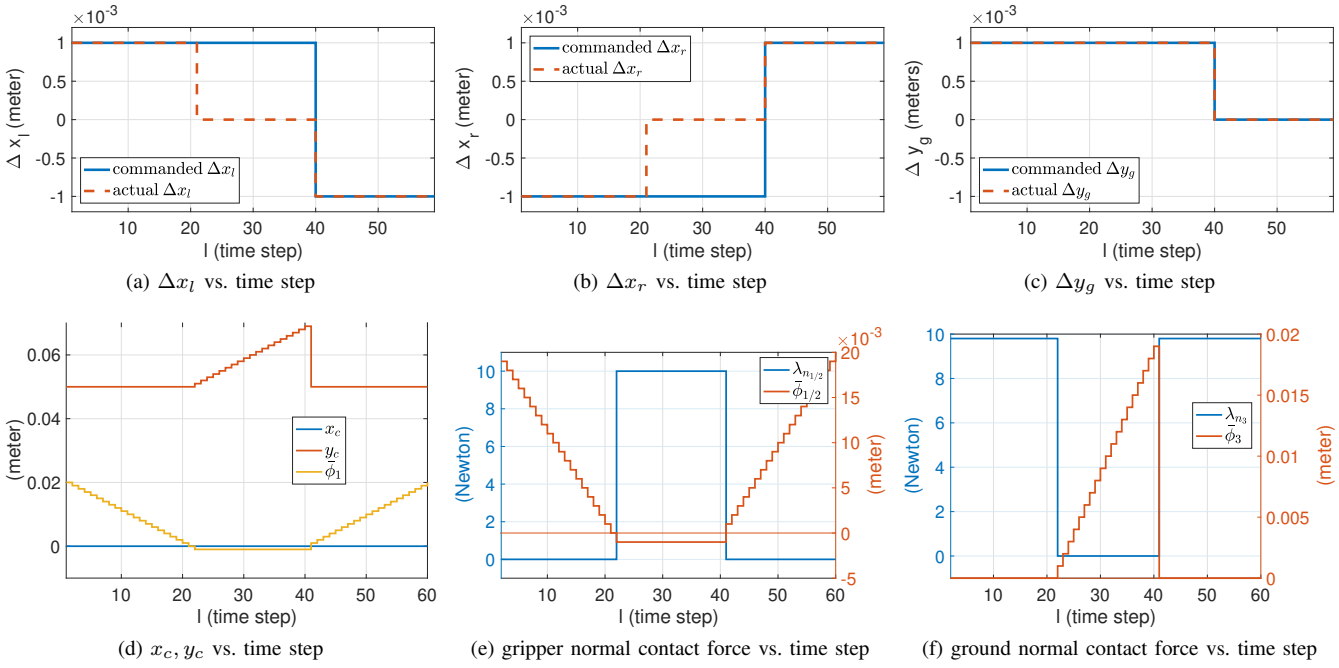

(a) Δx_l vs. time step (b) Δx_r vs. time step (c) Δy_g vs. time step

(d) x_c, y_c vs. time step (e) gripper normal contact force vs. time step (f) ground normal contact force vs. time step

Fig. 5: Cylinder-gripper system simulation result using MIQP

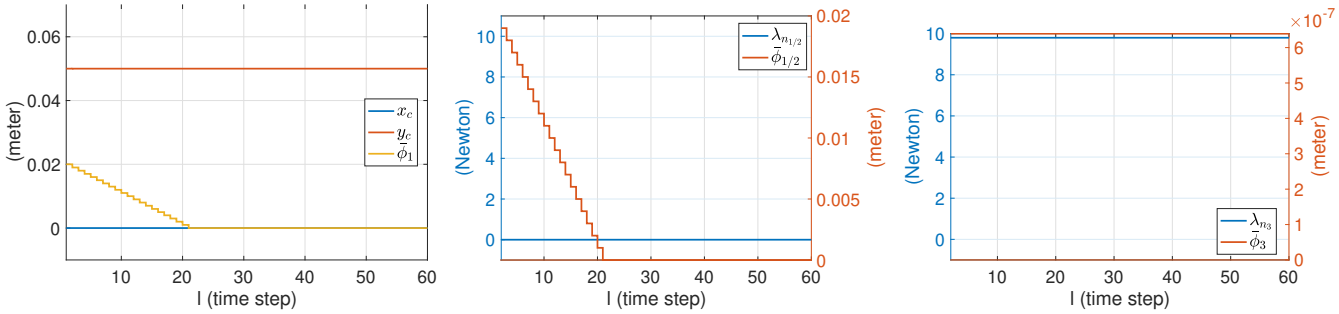

(a) x_c, y_c vs. time step (b) gripper normal contact force vs. time step (c) ground normal contact force vs. time step

Fig. 6: Cylinder-gripper system simulation result using LCP

in Section I: a parallel-jaw gripper picking up a cylinder of radius r. The 2D gripper-cylinder system is defined in Figure 4a: gravity points in the negative y direction; the cylinder has mass $m = 1\text{kg}$ and radius $r = 0.05\text{m}$; the fingers are parallel to the y-axis, and can translate in the x direction independently, but can only translate together in the y direction; the coefficient of friction for all contacts is $\mu = 0.5$. Simulation of this relatively simple system is implemented in MATLAB with Gurobi [19] as the MIQP solver.

The unactuated DOFs are $q_u = [x_c \quad y_c]^T$, where x_c and y_c are the x and y coordinates of the CG of the cylinder, respectively. The actuated DOFs are $q_a = [x_l \quad x_r \quad y_g]^T$, where x_l is the x-coordinate of the left finger, x_r the x-coordinate of the right finger, and y_g the height of the fingertips. To keep the evaluation of ϕ simple, we further assume that $y_g(t) < y_c(t)$ whenever the cylinder and the fingers are in contact. In addition, $v = \dot{q}$, therefore $J_*^v = J_*^q$.

As defined in Figure 4b, the distance function ϕ is

$$\phi = \begin{pmatrix} \phi_1 \\ \phi_2 \\ \phi_3 \end{pmatrix} = \begin{pmatrix} x_c - x_l - r \\ x_r - x_c - r \\ y_c - r \end{pmatrix}. \tag{24}$$

The velocities corresponding to the tangent vectors in Figure 4b are

$$\begin{aligned} &\nu_{11} = \nu_{21} = \dot{y}_c - \dot{y}_g, \\ &\nu_{31} = \dot{x}_c, \\ &\nu_{12} = -\nu_{11}, \nu_{22} = -\nu_{21}, \nu_{32} = -\nu_{31}. \end{aligned} \tag{25}$$

The normal and tangential Jacobians are

$$J_n^{q_u} = \begin{pmatrix} 1 & 0 \\ -1 & 0 \\ 0 & 1 \end{pmatrix}, J_n^{q_a} = \begin{pmatrix} -1 & 0 & 0 \\ 0 & 1 & 0 \\ 0 & 0 & 0 \end{pmatrix} \tag{26}$$

$$J_f^{q_u} = \begin{pmatrix} 0 & 1 \\ 0 & -1 \\ 0 & 1 \\ 0 & -1 \\ 1 & 0 \\ -1 & 0 \end{pmatrix}, J_f^{q_a} = \begin{pmatrix} 0 & 0 & -1 \\ 0 & 0 & 1 \\ 0 & 0 & -1 \\ 0 & 0 & 1 \\ 0 & 0 & 0 \\ 0 & 0 & 0 \end{pmatrix} \tag{27}$$

The other matrices used in the optimization problem (23) are

$$E = \begin{pmatrix} 1 & 0 & 0 \\ 1 & 0 & 0 \\ 0 & 1 & 0 \\ 0 & 1 & 0 \\ 0 & 0 & 1 \\ 0 & 0 & 1 \end{pmatrix}, U = \begin{pmatrix} 0.5 & 0 & 0 \\ 0 & 0.5 & 0 \\ 0 & 0 & 0.5 \end{pmatrix}. \tag{28}$$

The initial configuration of the system is $x_c(0) = 0$, $y_c(0) = r = 0.05$, $x_l(0) = -r - 0.02 = -0.07$, $x_r(0) = r + 0.02 = 0.07$. The system is simulated for 60 steps with a step size $h = 0.01$s. The gripper is commanded to move up and squeeze during the first 39 steps, and then stop moving up and release until the end of the simulation. Values of the velocity command are as follows:

$$\dot{\bar{q}}_a = \begin{pmatrix} \dot{x}_l \\ \dot{x}_r \\ \dot{y}_g \end{pmatrix} = \begin{cases} [0.1, -0.1, 0.1]^T & \text{if } l \leq 39 \\ [-0.1, 0.1, 0]^T & \text{if } l > 39 \end{cases}. \tag{29}$$

The stiffness consant K is chosen to ensure that the total friction force is able to balance gravity. In this example, $K = 10\text{N}/(0.1\text{m/s} \times 0.01\text{s}) = 10^4\text{N/m}$.

Following the velocity command, the fingers touch the cylinder surface ($\phi_1 = \phi_2 = 0$) at step 21. As the fingers are commanded to continue squeezing, the x-direction velocity command is not strictly followed in order to avoid penetration (Figure 5a and 5b). In contrast, the velocity command in the y-direction is perfectly followed (Figure 5c) because it does not cause penetration.

Meanwhile, a lower bound is added to the normal forces between the the cylinder and the fingers after detecting hypothetical penetration (Figure 5e). As a result, the object is picked up by the grippers, as shown in Figure 5d.

After being released from the grippers, the cylinder immediately teleports back to the table top (Figure 5d) because the cylinder has to always stay in equilibrium. Free-falling would violate the force balance constraint, and hence would not happen in quasistatic systems.

In comparison, simulation results using the LCP-based time-stepping scheme are also shown in Figure 6. This simulation is also implemented in MATLAB with LCPs solved by the PATH Solver [20]. As the velocity command (29) would lead to an infeasible LCP, the grippers are instead commanded to stop squeezing after touching the cylinder surface:

$$\dot{\bar{q}}_a = \begin{pmatrix} \dot{x}_l \\ \dot{x}_r \\ \dot{y}_g \end{pmatrix} = \begin{cases} [0.1, -0.1, 0.1]^T & \text{if } l \leq 20 \\ [0, 0, 0.1]^T & \text{if } l > 20 \end{cases}. \tag{30}$$

As shown in Figure 6b, the normal force between the gripper and the cylinder remains zero throughout the simulation. As a result, the cylinder stays on the table (Figure 6a, 6c) even though the gripper is constantly moving up.

B. 3D grasping and manipulation using a robotic arm

The simulator can also handle a more complex scenario where a 7-DOF robotic arm with a parallel-jaw gripper tries to pick up a 6-DOF cylinder from a table. Starting upright with the gripper widely open (Figure 7a), the arm first moves down to a pre-grasp position (Figure 7b). The gripper is then commanded to grasp the cylinder (Figure 7c). After being grasped, the object is lifted (Figure 7d) and moved through a trajectory that involves simultaneous translation and rotation (7e).

The cylinder-gripper-arm system is implemented in Drake [21], a C++ control and simulation toolbox. Drake includes a comprehensive set of tools commonly used in robotics, such as inverse kinematics (IK), rigid body kinematics and dynamics, which are used to generate robotic arm trajectories, evaluate signed distance functions and compute Jacobians.

Sometimes, using a large stiffness K on the right hand side of constraint (23f) leads to stiff optimizations that are numerically unstable. One way to circumvent this problem is to generate normal force lower bounds using $\bar{\phi}^l$, the hypothetical penetration from time step $l-1$, when constructing the MIQP (23) for time step l. Doing this results in a 1-time-step delay between making contact and applying normal force, but makes the optmization less stiff and easier to solve.

The trajectory in Figure 7 is 12 seconds long. With a time step $h = 0.005$s, 2400 MIQP's are solved throughout the entire simulation. To see how runtime scales with the number of binary variables, we also simulated the same arm trajectory using an object with a more complex contact geometry. By querying Gurobi's *Runtime* attribute after each solve, the time spent on solving the MIQP at each time step can be obtained. The Gurobi runtime statistics are summarized in Table I.

Object	No. of binary variables	Solver runtime per time step (ms)		
		Average	Worst	Standard deviation
Cylinder	36	2.7	11.8	0.83
Rounded box	72	6.6	118.7	9.7

TABLE I: MIQP solver (Gurobi) runtime statistics for two different models.

VI. Conclusion

In this work, we identified two drawbacks of the existing LCP-based quasistatic time-stepping scheme: the violation of non-penetration constraints caused by the velocity command and the existence of undesirable solutions to the force balance constraints. To overcome these issues, we reformulated the LCP as an MIQP, representing complementarity using the big-M method and adding an objective. Firstly,

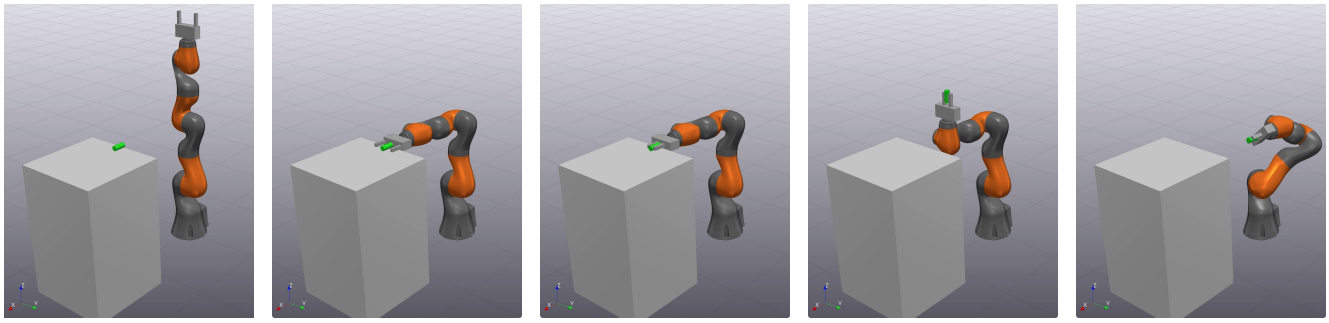

(a) Initial position (b) Pre-grasp position (c) Grasping cylinder (d) Picking up cylinder (e) Moving cylinder in 3D

Fig. 7: Grasping and manipulation using a robotic arm and a parallel gripper

non-penetration constraints can be satisfied by choosing an objective that minimizes the difference between the actual and commanded velocities. Secondly, by adding normal force lower bounds that are proportional to the hypothetical penetration, undesirable solutions with small normal forces can be removed. Finally, we illustrated the effectiveness of the MIQP reformulation with a simple 2D system, and demonstrated its ability to handle non-trivial simulations with a more complex 3D system.

SOURCE CODE

The source code for this work is part of Drake [21], and can be found at `https://github.com/RobotLocomotion/drake/blob/master/manipulation/dev`.

ACKNOWLEDGMENT

The authors would like to acknowledge the support from Air Force/Lincoln Laboratory award 7000374874; NASA award NNX16AC49A; Army Research Office award W911NF-15-1-0166 and Draper Laboratory Incorporated award SC001-0000001002. The views expressed in this paper are those of the authors themselves and are not endorsed by the funding agencies. The authors also thank Twan Koolen and Robin Deits for many helpful discussions and insights.

REFERENCES

[1] P. Song, V. Kumar, J. Trinkle, and J.-S. Pang, "A family of models for manipulation planning," in *Assembly and Task Planning: From Nano to Macro Assembly and Manufacturing, 2005.(ISATP 2005). The 6th IEEE International Symposium on*. IEEE, 2005, pp. 236–241.

[2] M. T. Mason, "Progress in nonprehensile manipulation," *The International Journal of Robotics Research*, vol. 18, no. 11, pp. 1129–1141, 1999.

[3] K. M. Lynch, H. Maekawa, and K. Tanie, "Manipulation and active sensing by pushing using tactile feedback." in *IROS*, 1992, pp. 416–421.

[4] M. T. Mason, "Mechanics and planning of manipulator pushing operations," *The International Journal of Robotics Research*, vol. 5, no. 3, pp. 53–71, 1986.

[5] K. M. Lynch and M. T. Mason, "Stable pushing: Mechanics, controllability, and planning," *The International Journal of Robotics Research*, vol. 15, no. 6, pp. 533–556, 1996.

[6] R. D. Howe and M. R. Cutkosky, "Practical force-motion models for sliding manipulation," *The International Journal of Robotics Research*, vol. 15, no. 6, pp. 557–572, 1996.

[7] F. R. Hogan and A. Rodriguez, "Feedback control of the pusher-slider system: A story of hybrid and underactuated contact dynamics," *arXiv preprint arXiv:1611.08268*, 2016.

[8] J. Zhou, J. A. Bagnell, and M. T. Mason, "A fast stochastic contact model for planar pushing and grasping: Theory and experimental validation," in *Robotics: Science and systems XIII*, 2017.

[9] D. Stewart and J. C. Trinkle, "An implicit time-stepping scheme for rigid body dynamics with coulomb friction," in *Robotics and Automation, 2000. Proceedings. ICRA'00. IEEE International Conference on*, vol. 1. IEEE, 2000, pp. 162–169.

[10] M. Anitescu and F. A. Potra, "Formulating dynamic multi-rigid-body contact problems with friction as solvable linear complementarity problems," *Nonlinear Dynamics*, vol. 14, no. 3, pp. 231–247, 1997.

[11] M. Posa, C. Cantu, and R. Tedrake, "A direct method for trajectory optimization of rigid bodies through contact," *The International Journal of Robotics Research*, vol. 33, no. 1, pp. 69–81, 2014.

[12] S. Goyal, A. Ruina, and J. Papadopoulos, "Planar sliding with dry friction part 1. limit surface and moment function," *Wear*, vol. 143, no. 2, pp. 307–330, 1991.

[13] J. Zhou, R. Paolini, J. A. Bagnell, and M. T. Mason, "A convex polynomial force-motion model for planar sliding: Identification and application," in *Robotics and Automation (ICRA), 2016 IEEE International Conference on*. IEEE, 2016, pp. 372–377.

[14] J. Trinkle, S. Berard, and J. Pang, "A time-stepping scheme for quasistatic multibody systems," in *Assembly and Task Planning: From Nano to Macro Assembly and Manufacturing, 2005.(ISATP 2005). The 6th IEEE International Symposium on*. IEEE, 2005, pp. 174–181.

[15] E. G. Gilbert, D. W. Johnson, and S. S. Keerthi, "A fast procedure for computing the distance between complex objects in three-dimensional space," *IEEE Journal on Robotics and Automation*, vol. 4, no. 2, pp. 193–203, 1988.

[16] V. Duindam, "Port-based modeling and control for efficient bipedal walking robots," Ph.D. dissertation, University of Twente, 2006.

[17] R. M. Murray, *A mathematical introduction to robotic manipulation*. CRC press, 2017.

[18] A. K. Valenzuela, "Mixed-integer convex optimization for planning aggressive motions of legged robots over rough terrain," Ph.D. dissertation, Massachusetts Institute of Technology, 2016.

[19] Gurobi Optimization, Inc., "Gurobi optimizer reference manual," 2017. [Online]. Available: http://www.gurobi.com/

[20] S. P. Dirkse and M. C. Ferris, "The path solver: a nommonotone stabilization scheme for mixed complementarity problems," *Optimization Methods and Software*, vol. 5, no. 2, pp. 123–156, 1995.

[21] R. Tedrake and the Drake Development Team, "Drake: A planning, control, and analysis toolbox for nonlinear dynamical systems," 2016. [Online]. Available: http://drake.mit.edu